Materials Transactions, Vol. 44, No. 5 (2003) pp. 806 to 810
Special Issue on Solidification Science and Processing for Advanced Materials

Direct Crystallization of the $Nd_2Fe_{14}B$ Peritectic Phase by Containerless Solidification in a Drop Tube

Shunpei Ozawa[1], Mingjun Li[1], Suguru Sugiyama[2], Itaru Jimbo[2] and Kazuhiko Kuribayashi[1]

[1]*The Institute of Space and Astronautical Science, Sagamihara 229-8510, Japan*
[2]*Department of Metallurgical Engineering, Tokai University, Hiratsuka 259-1292, Japan*

$Nd_2Fe_{14}B$ molten alloy droplets were containerlessly solidified using a 25 m drop tube. The relationship between the sample diameter and the microstructure was investigated. The diameter of the resultant spherical samples was in range of 150 to 2000 µm. When sample diameter was larger than 500 µm, the microstructure of the spherical sample consisted of the α-Fe phase embedded in matrix of the $Nd_2Fe_{14}B$ phase within entire sections. In the spherical sample with diameter of 400 µm, the microstructures consisted of two regions, one was columnar grains of the $Nd_2Fe_{14}B$ phase and the other was α-Fe phase embedded in matrix of the $Nd_2Fe_{14}B$ phase. The columnar $Nd_2Fe_{14}B$ region expanded as the sample diameter decreased from 400 to 350 µm. When sample diameter reduced to 250 µm, the microstructure of a spherical sample consisted of the pure dendritic $Nd_2Fe_{14}B$ phase without any α-Fe phase.

(Received November 21, 2002; Accepted February 17, 2003)

Keywords: *containerless solidification, undercooling, direct crystallization, neodymium–iron–boron*

1. Introduction

Neodymium–iron–boron (Nd–Fe–B) permanent magnets are one of the highest performance magnets. It has been reported[1)] that the Nd–Fe–B magnets can yield the maximum energy products of more than 444 kJm^{-3}. This value is over 10 times larger than that of ferrite magnets that are widely applied at present. Therefore, the production volume of the Nd–Fe–B magnets will increase due to the expanding needs in various applications such as computer and electric devices.

The superiority of the magnets originates from the $Nd_2Fe_{14}B$ intermetallic compound that exhibits a large saturation magnetization and a high anisotropy field.[2,3)] According to the Nd–Fe–B ternary alloy phase diagram, the $Nd_2Fe_{14}B$ phase is formed via the peritectic reaction from liquid phase and primary iron phase.[4)] Therefore, the primary iron phase always remains between the $Nd_2Fe_{14}B$ phase in alloy ingots due to the nature of peritectic reaction.[5,6)] The primary iron phase transforms to the soft magnetic α-Fe phase at room temperature, which deteriorates the hard magnetic property of the Nd–Fe–B magnets. Thus, it is crucial to reduce the amount of the primary iron phase in Nd–Fe–B alloy ingots.

A large undercooling is one of the most promising alternatives for yielding peritectic compounds directly from a melt. The most common technique to obtain a large undercooling is the rapid solidification processing such as melt-spinning or splat-quenching.[7,8)] Furthermore, it has been reported that an undercooling can be achieved by containerless solidification.[9,10)] In the containerless technique, a bulk liquid material may experience a large undercooling prior to solidification because of the absence of container wall that may act as heterogeneous nucleation sites.

In this study, an Nd–Fe–B spherical alloy with the stoichiometric $Nd_2Fe_{14}B$ composition was produced by containerless solidification processing in a drop tube of 25 m in height. It is expected that the molten alloy droplets experience a large undercooling prior to solidification by drop tube processing. Such a large undercooling may favor the direct crystallization of the $Nd_2Fe_{14}B$ hard magnetic phase from the undercooled melt. The purpose of this study is to investigate the relationship between the sample size and the microstructure. The particular interest in the investigation was to confirm the critical diameter of a spherical sample, in which direct crystallization of the $Nd_2Fe_{14}B$ phase can be achieved without the primary iron phase.

2. Experimental Procedure

Figure 1 shows a schematic diagram of the drop tube experiment. Small segments of Nd–Fe–B alloy ingots with stoichiometric composition of $Nd_2Fe_{14}B$ were charged in a

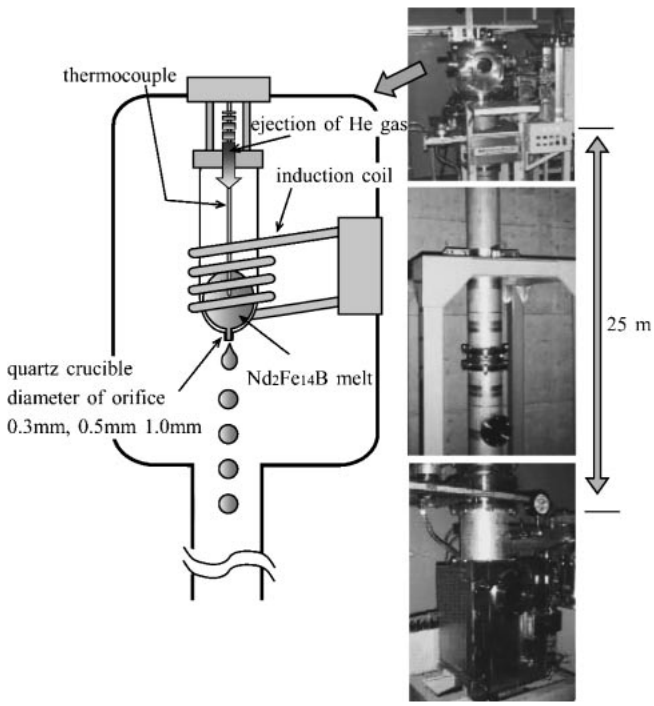

Fig. 1 Schematic diagram of the drop tube experiment.

quartz glass crucible with an orifice from 0.3 to 1.0 mm in diameter at the bottom. The quartz crucible with ingots was fixed in a chamber at the top of the drop tube. The drop tube was evacuated to 1×10^{-3} Pa and backfilled with 99.999% helium. The ingots were induction heated up to 1650 K that is about 100 K above the equilibrium liquidus temperature. The temperature of the melt was monitored by a thermocouple encased in a quartz glass sheath placed at the center of the sample. The molten alloy was ejected into the drop tube through the orifice by controlling the helium pressure, and shaped into comparatively uniform droplets continuously. The rapid solidification of the droplets was accomplished during their free fall in a containerless state. The sample accumulated at the bottom of the drop tube was spherical grain. The resultant samples were sifted into various groups according to sample diameter, ranging from 100 to 2000 μm with regard to the nozzle diameter and ejection pressure.

After spherical samples were polished and etched in 1% Nital, the microstructures and accurate diameter of the spherical samples were examined under scanning electron microscope (SEM) equipped with an electron probe micro-analyzer (EPMA) for analyzing chemical composition. The phases of the samples were identified by powdered X-ray diffraction (XRD) using Cu-K_α radiation at room temperature.

3. Results and Discussion

The spherical samples had a metallic surface in spite of a high oxidation tendency of the neodymium in the alloy. In the drop tube experiment, the melt solidifies without the container wall that may act as the heterogeneous nucleation site. Moreover, the reduction of the number of the potential heterogeneous nuclei in a fine droplet is favorable to enhance the undercooling level. Therefore, it is important to examine the influence of sample diameter on the phase selection and microstructure formation. It has been reported that a number of metals and alloys can experience an undercooling ΔT of $0.2 \times T_L$ prior to solidification.[11,12] When it is assumed that the $Nd_2Fe_{14}B$ melts experience an undercooling of $0.2 \times T_L$ prior to solidification, the free fall distance as a function of the sample diameter is shown in Fig. 2. This value is estimated by the following equations;

$$dT/dt = -6/(\rho C_p d)[h(T - T_0) + \sigma_{SB}\varepsilon(T^4 - T_0^4)] \quad (1)$$

$$dV/dt = g(\rho - \rho_g)/\rho_g - 3/4 D_r \rho (V^2/\rho d) \quad (2)$$

$$h = Kg/d(2.0 + 0.3 Pr^{0.33} Re^{0.6}) \quad (3)$$

$$D_r = 24/Re \quad (Re < 1) \quad (4)$$

$$D_r = (0.55 + 4.8/Re^{1/2})^2 \quad (1 < Re < 10^4) \quad (5)$$

where d is the diameter of droplets, ρ and ρ_g are the density of the droplet and gas, C_p is the specific heat of the droplet, h is heat transfer coefficient, T and T_0 are the melt temperature and ambient temperature, σ_{SB} is Stefan-Boltzmann constant, ε is the droplet surface hemispherical total emissivity, g is the gravitational acceleration, D_r is the drag coefficient, V is the relative velocity between the droplet and the gas and, K_g is thermal conductivity of the gas.[13] The physical properties used in the estimation are listed in Table 1. Maximum

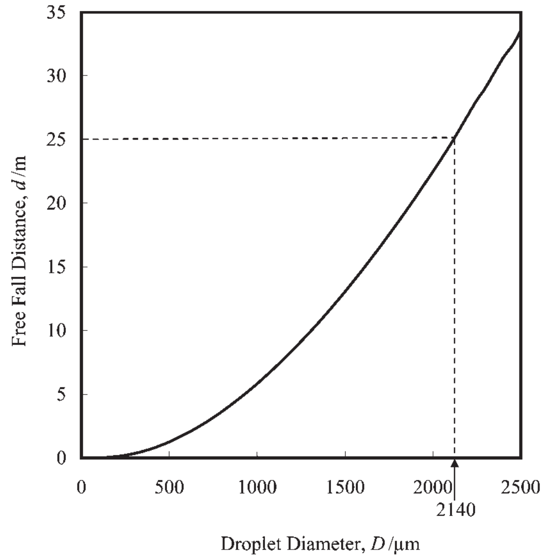

Fig. 2 Free fall distance as a function of the sample diameter.

Table 1 Physical properties used in the theoretical calculation in Fig. 2.

Parameter	Unit	Value
C_p	$Jkg^{-1}K^{-1}$	502
T	K	1650
T_0	K	300
ρ	kgm^{-3}	7600
ρ_g	kgm^{-3}	0.1785
K_g	Pas^{-1}	0.1422
e	—	0.1
g	ms^{-2}	9.8

diameter of the melt which can experience the undercooling of $0.2 \times T_L$ during free fall in the drop tube is about 2150 μm. In this study, the spherical sample with 150 to 2000 μm in diameter is obtained. Hence, the molten $Nd_2Fe_{14}B$ droplet may experience such a large undercooling.

Figure 3 shows the XRD patterns of the spherical $Nd_2Fe_{14}B$ alloys with various diameters solidified during free fall in the drop tube. For comparison, the XRD pattern of the alloy ingot is also depicted. The XRD pattern of the alloy ingot is well indexed to tetragonal $Nd_2Fe_{14}B$ phase and the α-Fe phase. This indicates that the alloy ingot contains some α-Fe phase together with the $Nd_2Fe_{14}B$ phase. In the stoichiometric $Nd_2Fe_{14}B$ alloy, the α-Fe phase should coexist with other phase such as Nd phase and Fe_2B phase.[4] However, no detectable diffraction peaks of other phase can be found in the XRD pattern. When the diameter of the spherical sample is 2000 μm, the XRD pattern of the samples shows the diffraction peaks of the $Nd_2Fe_{14}B$ phase and the α-Fe phase as is the case of the ingot. Virtually the same XRD patterns are obtained from the spherical samples with 500 μm and 400 μm in diameter. This indicates that the spherical samples with diameter in range of 2000 to 400 μm contain some α-Fe phase together with the $Nd_2Fe_{14}B$ phase as in that alloy ingot. It is expected that the primary γ-Fe phase was transformed to the stable α-Fe phase. The primary iron phase was not completely transformed into the $Nd_2Fe_{14}B$ phase by the

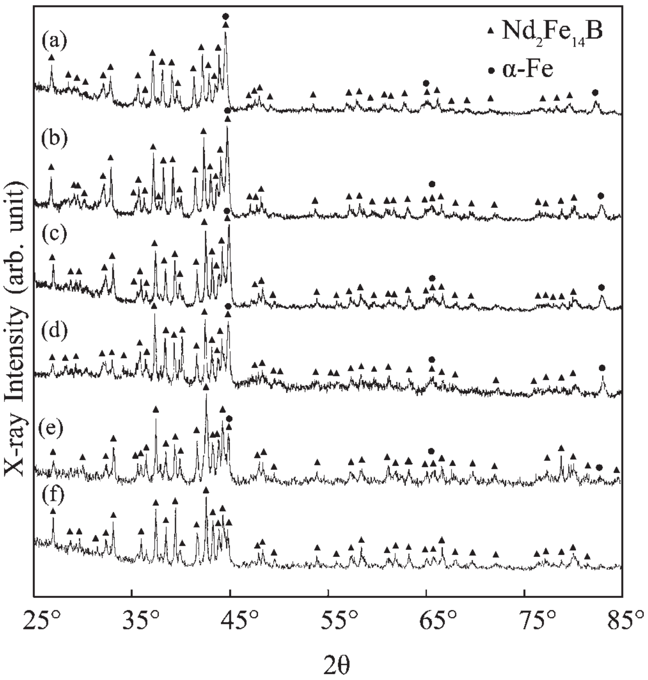

Fig. 3 XRD pattern of the $Nd_2Fe_{14}B$ alloy ingots (a) and (b), (c), (d), (e), and (f) depict the profiles of samples with 2000 μm, 500 μm, 400 μm, 350 μm, and 250 μm, respectively.

peritectic reaction and thus remained as the α-Fe phase in the spherical samples with diameter in range of 2000 to 400 μm. Although the diffraction peaks of the α-Fe phase can still be found in the XRD pattern of the spherical sample with 350 μm in diameter, the intensity of the diffraction peaks of the $Nd_2Fe_{14}B$ phase become slightly strong. This implies that the amount of the $Nd_2Fe_{14}B$ phase in the spherical sample with 350 μm in diameter increases, in short, the volume fraction of the α-Fe phase decreases. The XRD pattern of the sample with 250 μm in diameter shows only the diffraction peaks of the $Nd_2Fe_{14}B$ phase. No appreciable diffraction peaks of other phase are observed. This indicates that the spherical sample with 250 μm in diameter only consists of the $Nd_2Fe_{14}B$ phase.

Figure 4 shows the typical cross section microstructures of the spherical $Nd_2Fe_{14}B$ alloys with various diameters and further magnified microstructures at center position. The microstructure of the spherical sample with 500 μm in diameter consists of ''isolated fragmented dendrite'' embedding in matrix. EPMA study reveals that the fragmented dendrite and matrix are the α-Fe phase and the $Nd_2Fe_{14}B$ phase, respectively. Schwarz *et al.* have reported that such a fragmentation is resulted in a comparatively low cooling rate.[14] Even though the XRD studies does not confirm the existence of any other phase, the EPMA studies reveals that the grain boundary is Nd-rich phase. The volume fraction of this Nd-rich phase is so small that it is beyond the detectable limit of XRD.

In the spherical sample with diameter of 400 μm, the microstructure consists of two regions though almost the same microstructure is still observed at about 10 percent of the spherical samples. One is columnar grains together with grain boundary and the other is fragmented dendrites embedding in the matrix as that evidenced in the spherical samples with 500 μm in diameter. On the other hand, the columnar grains and grain boundaries were the $Nd_2Fe_{14}B$ phase and Nd-rich phase, respectively. When the $Nd_2Fe_{14}B$ phase is formed by peritectic reaction, it surrounds the primary iron phase and prevents further peritectic reaction. As a result, the primary iron phase always remains in the resultant $Nd_2Fe_{14}B$ phase.[5,6] However, no primary iron phase was observed in the current columnar $Nd_2Fe_{14}B$ grains. Similar columnar grains of $Nd_2Fe_{14}B$ phase can be observed in the microstructures of the Nd–Fe–B alloys solidified from the undercooled melt.[6] Hence, the $Nd_2Fe_{14}B$ columnar grains may be formed directly from the undercooled melt. As a diameter of the droplet is decreased, the probability for a droplet to contain potential catalytic site for heterogeneous nucleation is reduced and the cooling rate increases. Thus, the undercooling level may be enhanced by reduction of the sample diameter. Even if a number of droplets experience a large undercooling, it is expected that

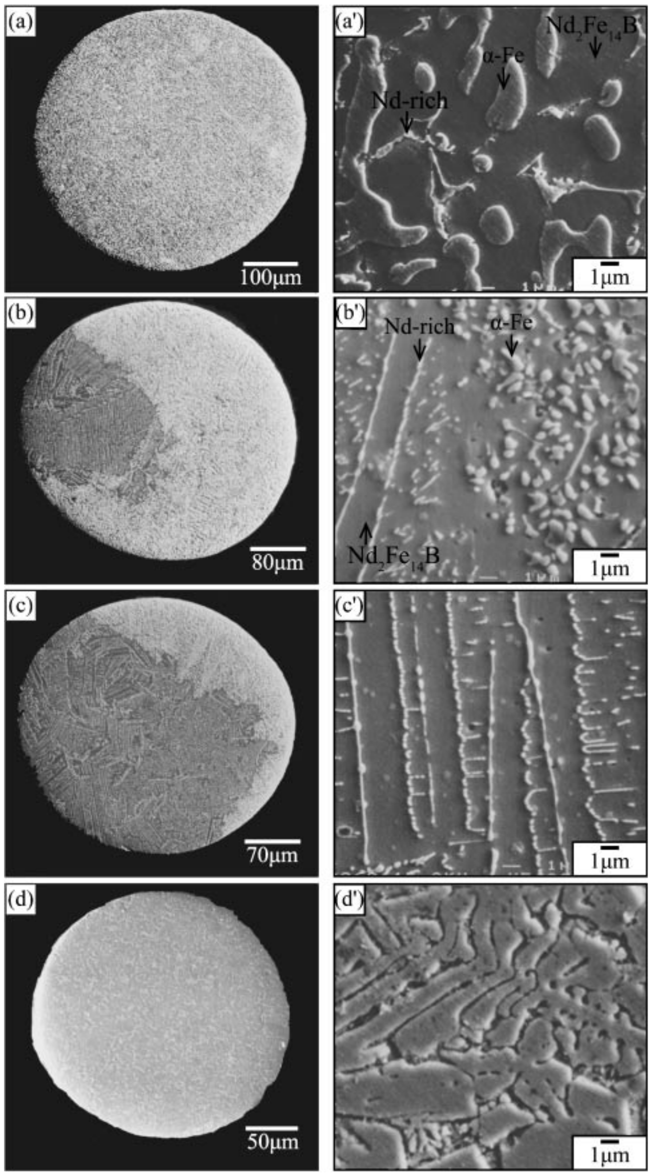

Fig. 4 Cross sectional microstructures of $Nd_2Fe_{14}B$ alloy with (a) 500 μm, (b) 400 μm, (c) 350 μm, and (d) 250 μm in diameter. (a'), (b'), (c') and (d') are further magnified microstructures of those at the enter, respectively.

some droplets do not experience such a large undercooling because potential heterogeneous nuclei should exist somewhere. Thus, about 10 percent of the sample with 400 μm in diameter may consist of the α-Fe and matrix. It has been reported that $Nd_2Fe_{14}B$ alloy solidified from the melt with the undercooling level of about 165 K mainly consists of $Nd_2Fe_{14}B$ phase.[15)] Therefore, the undercooling level that the spherical sample with 400 μm experiences may be lower than 165 K. The undercooling level of the spherical sample with 400 μm in diameter may not be sufficient as a heat sink to achieve the direct growth of the $Nd_2Fe_{14}B$ completely. In spite of the fact that about 10 percent samples consist of the α-Fe dendrite and $Nd_2Fe_{14}B$ matrix as similar case of the sample with 400 μm diameter, the region that consisted of columnar $Nd_2Fe_{14}B$ grains and grain boundary expands in the microstructure of the remainder spherical sample with 350 μm in diameter. The enhancement of the undercooling level due to the decrease of the diameter of the spherical sample must be responsible for such expansion of the $Nd_2Fe_{14}B$ columnar region. Two possibilities arise for the formation of the microstructure of two different region, as shown in Figs. 4(b') and (c'). The first is that the γ-Fe phase and the $Nd_2Fe_{14}B$ phase nucleate separately within one droplet almost simultaneously. Then two phases start to grow and from different microstructures. The second is that the $Nd_2Fe_{14}B$ phase will nucleate first and then begin to grow. Due to the pronounced sluggish kinetics in growth, the released crystallization heat may lower the interface undercooling and thus the growth of $Nd_2Fe_{14}B$ phase will be terminated. At this lower undercooling, the growth of iron phase will be predomination and then followed by a peritectic reaction. This solidification mode can also yield two different regions, as observed in Figs. 4(b') and (c').

In the spherical sample whose diameter is reduced to 250 μm, the microstructure consists of dendrites. No other microstructures can be observed in all samples with 250 μm in diameter. Although the morphology is different from the $Nd_2Fe_{14}B$ columnar grains in the spherical sample with 400 μm and 350 μm in diameter, EPMA study reveals that the dendrite grain is $Nd_2Fe_{14}B$ phase. This indicates that the critical diameter for obtaining the $Nd_2Fe_{14}B$ alloy without the α-Fe phase is in range of 250 μm and 350 μm, which coincides with the value reported by Gao and Wei.[16)] It is well known that dendrite is formed by continuous growth of a primary phase. Moreover, any α-Fe phase is not observed in the $Nd_2Fe_{14}B$ dendrites. Therefore, it is expected that the direct crystallization of the $Nd_2Fe_{14}B$ phase is completely achieved in the spherical sample with 250 μm in diameter. If such a direct growth of the $Nd_2Fe_{14}B$ phase is due to a large undercooled melt, the sample without the undercooling should be obtained as is the case of the sample with 400 μm and 350 μm in diameter. However, no microstructure that consists of $Nd_2Fe_{14}B$ and α-Fe is observed in all the samples with 250 m in diameter. This hints that the direct growth of the $Nd_2Fe_{14}B$ phase in the spherical sample with diameter less than 250 μm is not due to a large undercooling. The cooling rate of the sample is enhanced as the sample diameter decreases; the estimated cooling rate of the spherical sample with 250 μm in diameter is high value of 1.3×10^4 K/s. Therefore, it is expected that the direct growth of the $Nd_2Fe_{14}B$ phase in the spherical sample with 250 μm in diameter strongly depends on the high cooling rate rather than undercooling level. High cooling rate may suppress the primary growth of γ-Fe phase. It has been reported that a metastable $Nd_2Fe_{17}B_x$ is formed from undercooled Nd–Fe–B system melts.[17,18)] However, no evidence of the metastable phase was observed in this study. The dendrite arm spacing of $Nd_2Fe_{14}B$ phase is about 2.2 μm. This value is comparable to that in the strip cast Nd–Fe–B alloy, which is used for sintered magnets with high performance.[19)] Thus, a drop tube is well promising for the production of $Nd_2Fe_{14}B$ alloys without the α-Fe phase.

4. Conclusion

Spherical Nd–Fe–B alloy ingots with the stoichiometric composition of $Nd_2Fe_{14}B$ were produced by a containerless solidification processing in a 25-m drop tube. The relationship between the sample size and microstructure was investigated and then, the critical diameter for forming the $Nd_2Fe_{14}B$ phase without the α-Fe phase was determined. The microstructure of the sample with 500 μm in diameter consisted of the "fragmented dendrites" of the α-Fe phase and matrix of the $Nd_2Fe_{14}B$ phase. The growth of primary iron phase is due to a low cooling rate and low undercooling level. In the sample diameter was 400 μm and 350 μm, almost all the microstructure consisted two regions, one is primary $Nd_2Fe_{14}B$ columnar grains and the other is "fragmented dendrites" of the α-Fe phase in matrix of the $Nd_2Fe_{14}B$ phase. The region that consists of $Nd_2Fe_{14}B$ columnar grains expands as the sample diameter decreases from 400 to 350 μm. Such a direct growth of the $Nd_2Fe_{14}B$ columnar depends on the enhancement of the undercooling level. When sample diameter reduced to 250 μm, the microstructure consisted of only primary $Nd_2Fe_{14}B$ dendrites without the α-Fe phase. High cooling rate of the sample must be responsible for the primary $Nd_2Fe_{14}B$ dendrites without the α-Fe phase. The critical diameter for forming the $Nd_2Fe_{14}B$ phase without the α-Fe phase was in range of 250 μm and 350 μm.

Acknowledgments

This work was financially supported by a grant-in aid for Scientific Research from The Ministry of Education, Culture, Sports, Science and Technology. We also thank Dr. S. Hirosawa (Research and Development Center, Sumitomo Special Metals Co., Ltd JAPAN) for supplying the Nd–Fe–B alloy ingot. One of authors (M. Li) is grateful to Japan Society for the Promotion of Science (JSPS) for offering a JSPS fellowship.

REFERENCES

1) Y. Kaneko: the Sixteenth International Workshop on Rare-Earth Magnets and their Applications, ed. by H. Kaneko, M. Homma, M. Okada, (Sendai, Miyagi, 2000) 83–98.
2) N. C. Koon, B. N. Das, M. Rubinstein and J. Tyson: J. Appl. Phys. **57** (1985) 4091–4093.
3) C. Abache and Oesterreicher: J. Appl. Phys. **57** (1985) 4112–4114.
4) G. Schneider, E. T. Hening, G. Petzow and H. H. Stadelmaier: Z. Metallk. **77** (1986) 755–771.

5) S. Ozawa, J. Yoshizawa, T. Saito and T. Motegi: Mater. Trans., JIM **41** (2000) 1121–1124.
6) S. Ozawa, T. Saito, J. Yu and T. Motegi: J. Alloy. Compd. **322** (2001) 276–280.
7) J. J. Croat, J. F. Herbst, R. W. Lee and F. E. Pinkerton: J. Appl. Phys. **55** (1984) 2078–2082.
8) M. Li, K. Nagashio and K. Kuribayashi: J. Mater. Res. **17** (2002) 2026–2032.
9) K. Nagashio, Y. Takamura, K. Kuribayashi and Y. Shiohara: J. Cryst. Growth **200** (1999) 118–125.
10) K. Nagashio, K. Kuribayashi and Y. Shiohara: Acta Mater. **50** (2002) 3003–3012.
11) D. Turnbull: J. Chem. Phys. **20** (1952) 411–424.
12) D. Turnbull and R. E. Cech: J. Appl. Phys. **21** (1950) 804–810.
13) D. M. Herlach, R. F. Cochrane, I. Egry, H. J. Fecht and A. L. Greer: Int. Mater. Rev. **38** (1993) 273–347.
14) M. Schwarz, A. Karma, K. Eckler and D. M. Herlach: Phys. Rev. Lett. **73** (1994) 1380–1383.
15) S. Ozawa, H. Sato, T. Saito and T. Motegi: J. Appl. Phys. **91** (2002) 8831–8833.
16) J. Gao and B. Wei: J. Alloy. Compd. **285** (1999) 229–232.
17) J. Gao, T. Volkmann and D. M. Herlach: J. Alloy. Compd. **308** (2000) 296–300.
18) J. Gao, T. Volkmann and D. M. Herlach: Acta Mater. **50** (2002) 3003–3012.
19) W. Pei, C. He, F. Lian, G. Zhou and H. Yang: J. Magn. Magn. Mater. **239** (2002) 475–478.